Research article

Journal of Applied Toxicology

Received: 20 April 2016, Revised: 3 June 2016, Accepted: 4 June 2016 Published online in Wiley Online Library: 21 July 2016

(wileyonlinelibrary.com) DOI 10.1002/jat.3361

Pulmonary persistence of graphene nanoplatelets may disturb physiological and immunological homeostasis

Eun-Jung Park[a]*, Sang Jin Lee[b], Kyuhong Lee[b], Young Chul Choi[c], Byoung-Seok Lee[d], Gwang-Hee Lee[e] and Dong-Wan Kim[e]

ABSTRACT: Accumulated evidence suggests that chronic pulmonary accumulation of harmful particles cause adverse pulmonary and systemic health effects. In our previous study, most of the graphene nanoplatelet (GNP) remained in the lung until 28 days after a single instillation. In this study, we sought to evaluate the local and systemic health effect after a long pulmonary persistence of GNP. As expected, GNP remained in the lung on day 90 after a single intratracheal instillation (1.25, 2.5 and 5 mg kg^{-1}). In the lung exposed at the highest dose, the total number of cells and the percentage of lymphocytes significantly increased in the BAL fluid with an increase in both the number of GNP-engulfed macrophages and the percentage of apoptotic cells. A Th1-shifted immune response, the elevated chemokine secretion and the enhanced expression of cytoskeletal-related genes were observed. Additionally, the expression of natriuretic-related genes was noteworthy altered in the lungs. Moreover, the number of white blood cells (WBC) and the percentage of macrophages and neutrophils clearly increased in the blood of mice exposed to a 5-mg kg^{-1} dose, whereas total protein, BUN and potassium levels significantly decreased. In conclusion, we suggest that the long persistence of GNP in the lung may cause adverse health effects by disturbing immunological- and physiological-homeostasis of our body. Copyright © 2016 John Wiley & Sons, Ltd.

Additional supporting information may be found in the online version of this article at the publisher's web site.

Keywords: Graphene; nanoplatelets; immunotoxicity; immune regulation; physiology; antigen presentation

Introduction

Graphene is a single-atom-thick two-dimensional sheet having sp2-hybridized carbon atoms arranged hexagonally and has unique physicochemical properties, including a high surface area, extraordinary electrical and thermal conductivity and a high mechanical strength. Since the first isolation of graphene in 2004, different forms of graphene with various shapes, sizes, number of layers, chemical modifications and other characteristics have been developed for application in numerous areas, including semiconductors, electronics, energy storage, composite industries, tissue engineering, drug delivery and biomedicine (Geim, 2009; Novoselov, 2011; Ruiz *et al*., 2011; Kuila *et al*., 2013; Yang *et al*., 2013; Goenka *et al*., 2014; Kostarelos and Novoselov, 2014; Zhang *et al*., 2014a; Perrozzi *et al*., 2015). Thus, unintended or intended human exposure to graphene-based nanomaterials is expected to increase in the future, which has created the need to consider the safety of these nanomaterials. However, owing to the relatively latest isolation, information available about the health effects of graphene is very limited compared with the other carbon-based nanomaterials such as carbon nanotubes and carbon black. Moreover, to date, most studies on the toxicity of graphene and its derivatives used graphene oxide (GO), a highly oxidized form of chemically modified graphene, and reduced GO (rGO), the product obtained after treating GO under reducing conditions, because of better dispersibility and the stability of these forms in water and under physiological conditions compared with other graphene-based nanomaterials (Sanchez *et al*., 2012; Seabra *et al*., 2014).

Carbon-based nanomaterials, including single- and multi-walled carbon nanotubes, carbon black, fullerene and graphene, are almost chemically identical, and graphene has a smaller aspect ratio and a larger surface area relative to carbon nanotubes. Thus, some researchers predicted that graphene might not induce harmful biological responses similar to those associated with fibrous asbestos or carbon nanotubes (Ali-Boucetta *et al*., 2013; Bussy *et al*., 2013; Seabra *et al*., 2014; Zhang *et al*., 2014b). However, accumulating evidence demonstrate that graphene and its derivatives induce *in vitro* and *in vivo* toxicity via various mechanisms (Sanchez et al., 2012; Guo and Mei, 2014).

Inhalation is one of main entry routes for nanomaterials into the human body as well ingestion and dermal and biomedical application. Additionally, most of them are produced as powders which

*Correspondence: Eun-Jung Park, Myunggok Eye Research Institute, Konyang University, 685, Gasuwon-dong, Seo-Gu, Daejeon, 302-718, Korea.
E-mail: pejtoxic@hanmail.net

[a]Myunggok Eye Research Institute, Konyang University, Daejeon, Korea

[b]Inhalation Toxicology Center, Korea Institute of Toxicology, Korea

[c]Nano-Electron Creative Research Center, Electronics and Telecommunications Research Institute, Daejeon, Korea

[d]Toxicologic Pathology Center, Korea Institute of Toxicology, Daejeon, Korea

[e]School of Civil, Environmental, and Architectural Engineering, Korea University, Seoul, Korea

Journal of Applied Toxicology

are potentially inhalable materials, although there have been no reports of studies on exposure to air-bone graphene (and its derivatives) (Sanchez *et al.*, 2012). Moreover, the host's immune system efficiently maintains homeostasis by engulfing, digesting and subsequently cleaning up nanomaterials which enter into the body. According to the recently published reports, graphene and its derivatives may cause disease by disrupting the balance of the immune system (Schinwald *et al.*, 2012; Wang *et al.*, 2013; Shurin *et al.*, 2014; Park *et al.*, 2015a). For example, graphene nanosheets (1 mg kg^{-1}) induced Th2-type immune responses with the activation of interleukin-33 (IL-33) and ST2 receptors in the lung on day 1 after intravenous injection (Wang *et al.*, 2013). In contrast, GO (80 μg mice^{-1}, approximately 2.5 mg kg^{-1}) attenuated the Th2-type immune responses, decreased the accumulation of eosinophils and enhanced the macrophage influx in a murine model of asthma (Shurin *et al.*, 2014). Furthermore, our previous study showed that most of the graphene nanoplatelets (GNP, 2.5 and 5 mg kg^{-1}) remained in the lung for 28 days after a single intratracheal instillation and enhanced the secretion of granulocyte macrophage colony-stimulating factor (GM-CSF), macrophage chemoattractant protein (MCP)-1 and pro-inflammatory cytokines (Park *et al.*, 2015a). In this study, we hypothesized that the long persistence of GNP in the pulmonary system might show adverse health effects by impairing a host's immunological and physiological homeostasis. Considering that the upper limit dose volume of 5 ml kg^{-1} is recommended for installation in terms of animal welfare, we installated intratracheally the same dose of GNP (1.25, 2.5 and 5 mg kg^{-1}) as our previous study (Park *et al.*, 2015a), and then evaluated both locally and systemically the health effects on day 90 after instillation.

Materials and methods

Preparation of GNP

As previously reported (Park *et al.*, 2015a; Figure 1), GNP (Purity, 99.5%; Hanwha Nanotech, Daejeon, Korea) consisted of ~10 layers of graphene exhibited the thickness of ~3–4 nm and the lateral particle size of ~2 μm, based on transmission electron microscopy (TEM) analyzes. The GNP was loaded in phosphate-buffered saline (PBS) at a concentration of 1 mg ml^{-1} and sonicated for 1 h to achieve a stable dispersion of GNP (Supplementary Information Figure S1). The hydrodynamic diameter and surface charge of GNP dispersed in PBS were 325 ± 45.1 nm and −10.6 ± 0.7 mV, respectively, and the GNP was slightly aggregated in gamble's solution, an artificial lung fluid (506.5 ± 70.1 nm, Marques *et al.*, 2011).

Animal care and GNP treatment

Five-week-old male ICR mice (25–27 g, specific-pathogen free; OrientBio, Seongnam, Gyeonggi, Korea) were housed in our specific pathogen-free facility (23 ± 3 °C, 50 ± 10% humidity, 12 h light/dark cycle and ventilation of 10–20 times h^{-1}) for 1 week before the initiation of the study. Then, we intratracheally instilled GNP (1.25, 2.5 or 5 mg kg^{-1}, 140–150 μl mouse^{-1}, 16 mice per group) using a 24-gauge catheter under light tiletamine anesthesia as in our previous study (Park *et al.*, 2015a; Figure 2). The control group was treated with the same volume of PBS, and mice were euthanized on day 90 after a single instillation. The body weight was measured weekly, and significant changes in body weight after exposure were not observed during the experimental period (Supplementary Information Figure 2). The protocol for this study was assessed by the Institutional Animal Care and Committee (IACUC) of Ajou University (Suwon, Korea, IACUC No. 2013–0069) and was performed in accordance with the 'Guide for the Care and Use of Laboratory Animals', an Institution of Laboratory Animal Research (ILAR) publication.

Blood analysis

Whole blood was collected from the caudal vena cava, and a part was centrifuged at 3000 rpm (925 g) for 10 min to obtain serum for the immunoglobulin and biochemical analysis. Hematological and biochemical analysis were performed at the Neodin Veterinary Science Institute (Seoul, Korea) using a blood autoanalyzer (HemaVet850; CDC Technologies, Inc., Dayton, OH, USA) and a chemistry analyzer (BS-400; Mindray, Shenzhen, China), respectively.

BAL cell analysis

Bronchoalveolar lavage (BAL) fluids (1400–1700 μl) were obtained by cannulating the trachea and lavaging the lungs twice with cold

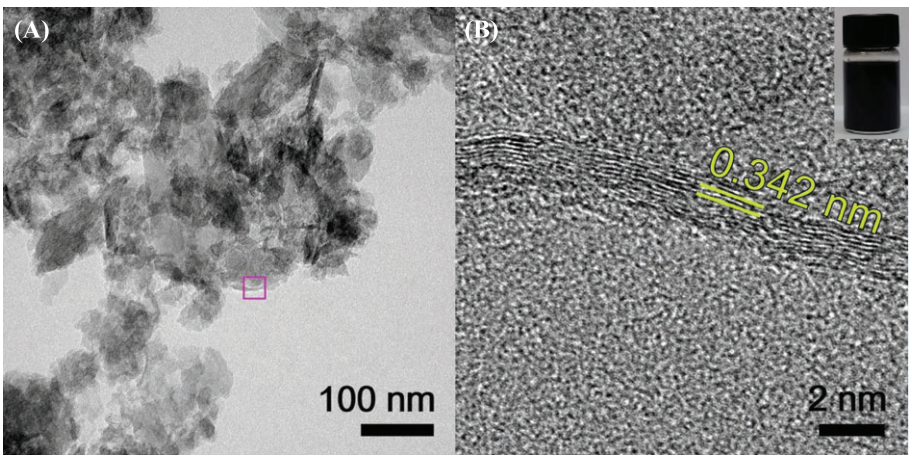

Figure 1. (A) Transmission electron microscopy (TEM) image of graphene nanoplatelet (GNP) and (B) a high-resolution TEM image of inset in (A) showing stacked GNP layers of an individual GNP.

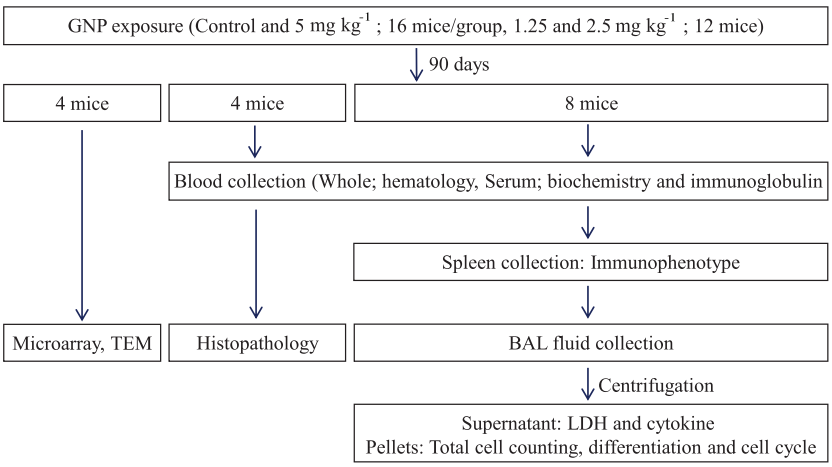

Figure 2. An experimental design.

sterile PBS (1 ml) on day 90 after a single instillation. After centrifuging at 1500 rpm (231 g) for 5 min, cell pellets were used for BAL cell (total cell counts and differentiation) and cell-cycle analysis, and the supernatants were used to measure the cytokine level (Park *et al.*, 2015b; Park *et al.*, 2016). BAL cell analysis was performed according to the standard operating procedure of Korea Institute of Toxicology, a good laboratory practice institute in Korea. Briefly, after removing red blood cells (RBC) from BAL cells using a VersaLyse (Beckman Coulter, Brea, CA, USA), the total number of cells in the BAL fluid was recorded using an automatic cell counter (ViCell XR, Beckman Coulter). Additionally, cell pellets were resuspended in PBS (200 ml) and placed onto slides using a Cytospin centrifuge (Thermo Shandon, Pittsburgh, PA, USA). Slides were fixed in methanol and stained with Diff-Quick (Sysmex Corporation, Tokyo, Japan). Then, different cell types (alveolar macrophages, neutrophils, lymphocytes and eosinophils) in the BAL fluid were quantified by their characteristic morphologies.

Cell cycle analysis

BAL cells were fixed with 70% ethanol. After washing with fluorescence-activated cell sorting (FACS) buffer, cells were treated with RNase A (200 $\mu g\,ml^{-1}$; Sigma-Aldrich, St. Louis, MO, USA) for 30 min, and then stained with propidium iodide (20 $\mu g\,ml^{-1}$; Sigma-Aldrich) for DNA labeling. The cell cycle was analyzed using

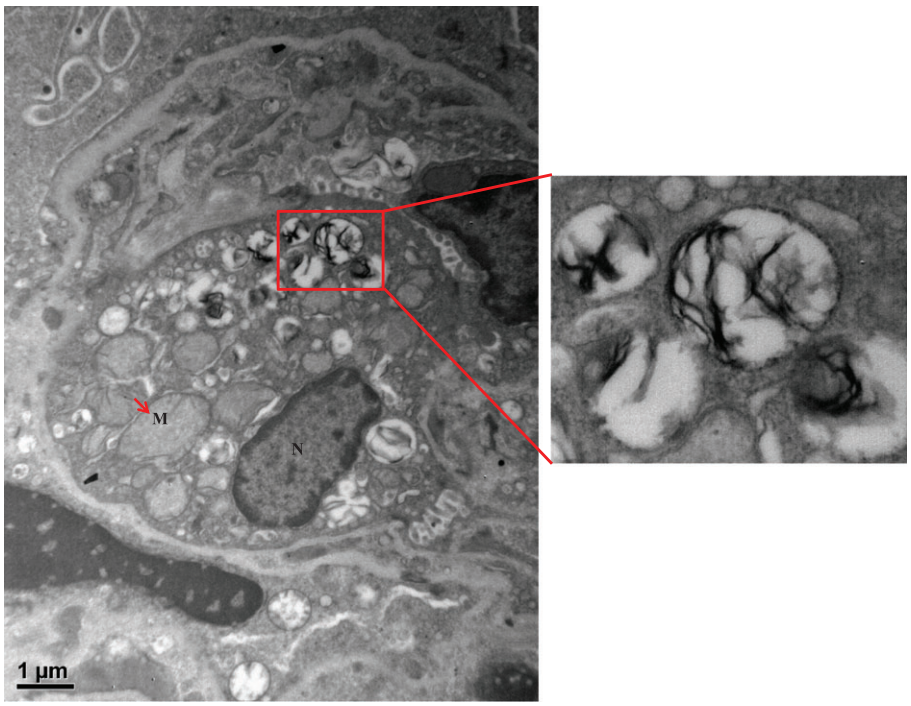

Figure 3. Fate of graphene nanoplatelet (GNP) in the lung tissues. A transmission electron microscopy (TEM) image was made with the lung tissues. We can find graphene nanoplatelet (GNP) within autophagosome-like vacuoles in a cell in the lung. M; mitochondria, N; nucleus.

Journal of Applied Toxicology

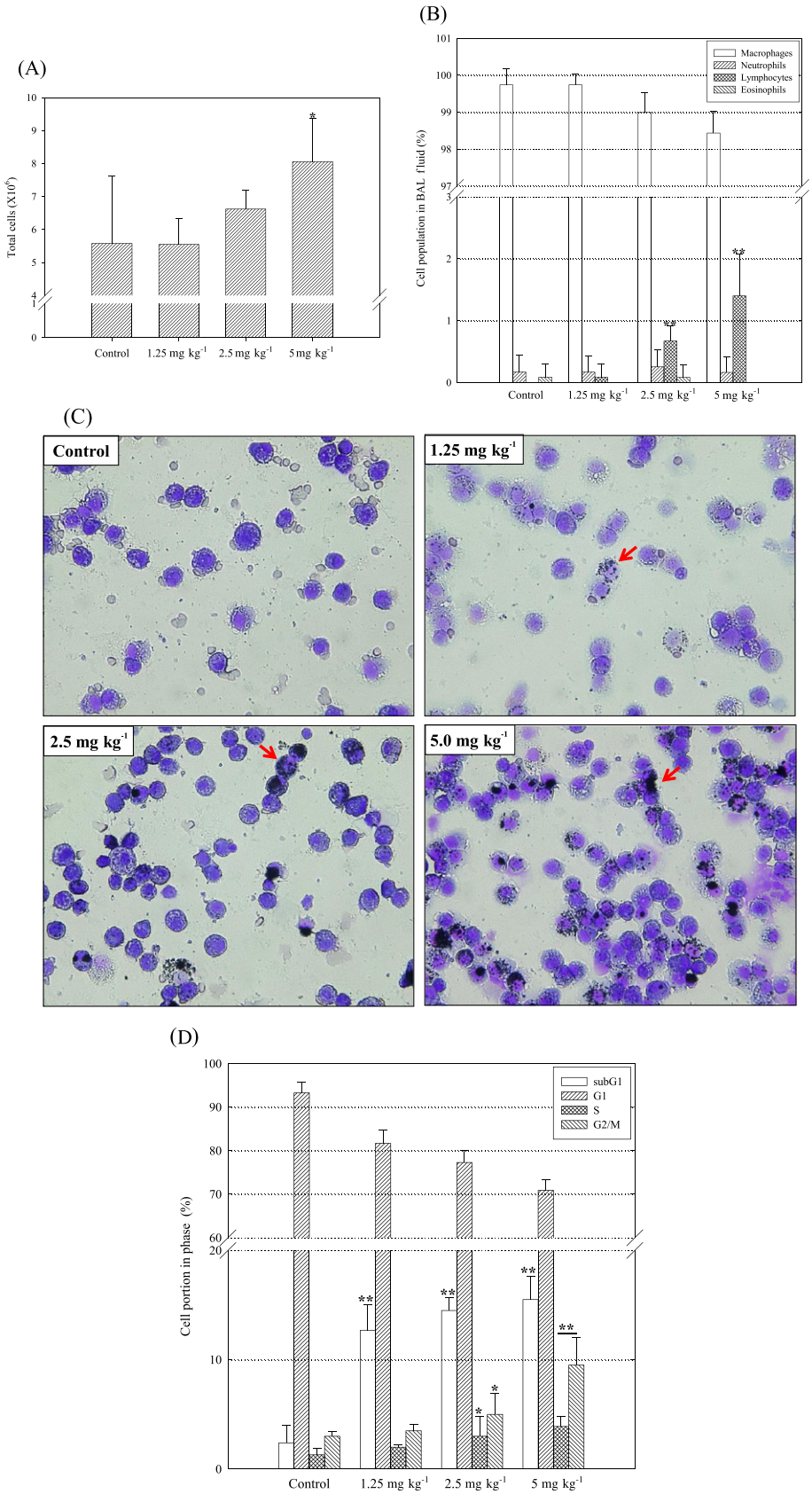

Figure 4. Changes in pulmonary cells after graphene nanoplatelet (GNP) accumulation. BAL fluids (eight mice per group) were collected on day 90 after a single intratracheal instillation, and centrifuged at 1,500 rpm for 5 min. The pellets were re-suspended in phosphate-buffered (PBS) and used for BAL cell analysis and cell-cycle analysis. Data are the mean ± standard deviation (SD). $^{*}P < 0.05$, $^{**}P < 0.01$. (A) The total cell number, (B) Differentiation of BAL cells, (C) Morphology of BAL cells. Arrows indicate GNP-laden macrophages. (D) Cell cycle analysis of BAL cells. 10 000 cells per sample were counted.

the FACSCalibur system and CellQuest software (BD Biosciences, Franklin Lakes, NJ, USA).

Cytokine assay

The concentrations of pro-inflammatory cytokines [IL-1β, tumor necrosis factor alpha (TNF)-α, IL-6], Th0 cytokine (IL-2), Th1-type cytokines [interferon (IFN)-γ and IL-12/IL-23], Th2-type cytokines (IL-4, IL-5, IL-10 and IL-13) and chemokines [macrophage inflammatory protein (MIP)-1 α, MCP-1, and GM-CSF] in BAL fluids and immunoglobulins (Ig, IgE, IgG, and IgM) in serum were determined using commercially available enzyme-linked immunosorbent assay kits (eBioscience, San Diego, CA, USA) according to the manufacturer's instructions. The reactions were stopped by adding 1 M H_3PO_4 solution, and the absorbance at 450 nm was measured using an ELISA reader (Molecular Devices, Sunnyvale, CA, USA). The concentration of each cytokine was calculated from the linear portion of a standard curve, which was generated under the same conditions.

FACS analysis

As reported previously, splenocytes were obtained by grounding the spleen (8 mice per group) in RPMI media containing fetal bovine serum (2%) and washed once with PBS (Park *et al.*, 2015b, 2016). After removing red cells with FACS lysis buffer, splenocytes were filtered using a 70 μm-pore size nylon mesh, and then were resuspended in FACS buffer. After blocking with Fc-block antibody to reduce non-specific binding, splenocytes were incubated with the fluorescence dye-conjugated antibodies: phycoerythrin (PE)-anti-CD11b, fluorescein isothiocyanate (FITC)-anti-CD11c, allophycocyanin (APC)-anti-MHC Class II (I-A/I-E), FITC-anti-CD3ε (for T cells), PE-anti-CD19 (for B cells), APC-anti-DX5 (for NK cells), PE-anti-CD4 (for helper T cells), FITC-anti-CD8 (for cytotoxic T cells), PE-anti-CD335 (NKp46, for NK cells), APC-anti-CD40, peridinin-chlorophyll proteins-anti-CD195, PE-anti-CD123 and FITC-anti-CD80 (B7–1) (eBioscience), APC-anti-CD86 (B7–2; BioLegend, Inc., San Diego, CA, USA), PE-anti-CXCR2 (R&D Systems, Inc., Minneapolis, MN, USA) for 30 min at 4 °C according to the manufacturer's instructions. After washing twice with FACS buffer, cells (10 000 per sample) were analyzed on an FACSCalibur (BD Biosciences) flow cytometer with CellQuest software.

Histopathological analysis and fate of GNP in the lung

Lung tissues (samples from four mice per group) were fixed by running 10% neutral buffered formalin into the lung and processed using routine histological techniques. After paraffin embedding, 3-μm sections were cut and stained with hematoxylin and eosin, and histopathological lesions were analyzed according to the standard operating procedures of the Korea Institute of Toxicology (Daejeon, Korea). Additionally, lung tissues were fixed in 2% glutaraldehyde in 0.1 M sodium cacodylate buffer (pH 7.2) for 2 h to observe the fate of GNP in the lung tissues (Park *et al.*, 2015a). Then, the tissues were stained for 30 min with 0.5% aqueous uranyl acetate, dehydrated in graded ethanol solutions and embedded in Spurr's resin. Thin sections were cut using an ultramicrotome (MT-X; RMC, Tucson, AZ, USA), stained with 2% uranyl acetate and Reynolds's lead citrate, and examined with a LIBRA 120 transmission electron microscope (Zeiss, Oberkochen, Germany) at an accelerating voltage of 80 kV.

Microarray analysis

To investigate changes in the gene profile after exposure to GNP, we extracted total RNA with the lung from mice in the control and the highest dose group (4 mice per group). Microarray analysis was performed by Macrogen Inc. (Seoul, Korea) using Illumina MouseRef-8 v2 Expression BeadChip (Illumina, Inc., San Diego, CA, USA) according to previously described methods (Park *et al.*, 2015a).

Statistical analysis

Data are the mean ± standard deviation (SD). Statistical significance of the changes after exposure to GNP was evaluated using the Student's *t*-test and one-way ANOVA followed by Tukey's posthoc comparison (GraphPad Software, San Diego, CA, USA). Statistical significant compared with the control was expressed as asterisks (*$P < 0.05$, **$P < 0.01$).

Results

Changes in BAL cells after persistence of GNP

Changes in pulmonary cell patterns after a long persistence of GNP were assessed by counting the number of total cells, macrophages, neutrophils, eosinophils and lymphocytes in BAL fluid. As expected, GNP remained in the lung on day 90 after a single instillation (Fig. 3). Additionally, as compared with the control, the total number of BAL cells significantly increased at a 5-mg kg^{-1} dose (Fig. 4A), and the percentage of lymphocytes was notably enhanced at doses of 2.5 and 5 mg kg^{-1} (Fig. 4B, Supplementary Information Table 1). Also, GNP-engulfed macrophages were remarkably observed in the treated group (Fig. 4C). Next, we performed cell cycle analysis to investigate BAL cell physiology. The percentage of the population in the subG1 region, which indicates apoptotic cells, was remarkably elevated in the GNP-treated mice accompanying arrest in the S and G2/M phase (Fig. 4D).

GNP altered Th1/Th2 cytokine balance in the lung

To evaluate the local immune response in the lung after pulmonary persistence of GNP, we measured the levels of the pro-inflammatory cytokines (IL-1β, TNF-α and IL-6), Th0 cytokine (IL-2), Th1-type cytokines (IFN-γ and IL-12/IL-23) and Th-2 type cytokines (IL-4, IL-5, IL-10 and IL-13) in BAL fluids (Fig. 5A). At the highest dose, GNP induced a general increase in cytokine secretion, particularly IL-12 (threefold higher than the control). In addition, the levels of MIP-1α (Th1-type chemokine), MCP-1 (Th2-type chemokine) and GM-CSF (white blood cell growth factor) were commonly elevated as compared with the control, especially MIP-1α (approximately 6.3 fold) and GM-CSF (2 fold) (Fig. 5B; Kim *et al.*, 2001; Campbell and HayGlass, 2000; Colantonio *et al.*, 2002; Fransico-Cruz *et al.*, 2014).

GNP altered the gene profile in the lung tissue without a remarkable pathological lesion

GNP-engulfed macrophages were observed within the alveoli lumen of GNP-instilled mice, but there were no remarkable pathological lesion associated with GNP persistence in the lung (Fig. 6). Meanwhile, as compared with the control, the expression of genes

Journal of Applied Toxicology

Table 1. A list of up-regulated genes after graphene nanoplatelet (GNP) accumulation. Lung tissues were collected from four mice per group for microarray analysis, and whole lung was then ground in RNA extract solution on ice. Lung tissues from two mice were pooled equivalently to make one sample for analysis ($n = 2$ per group). A list shows genes, which were up-regulated more than two-fold with statistical significance ($P < 0.05$)

RefSeq_NM	GeneSymbol	Fold	SD	DEFINITION
NM_177369.3	Myh8	39.2	3.6	myosin, heavy polypeptide 8, skeletal muscle, perinatal
NM_008725.2	Nppa	21.2	3.7	natriuretic peptide precursor type A
NM_009606.2	Acta1	21.2	2.6	actin, alpha 1, skeletal muscle
NM_009394.2	Tnnc2	20.2	2.2	troponin C2, fast
NM_016754.3	Mylpf	20.1	2.4	myosin light chain, phosphorylatable, fast skeletal muscle
NM_009416.3	Tpm2	16.5	2.0	tropomyosin 2, beta
NM_021285.1	Myl1	16.1	2.5	myosin, light polypeptide 1
NM_007504.2	Atp2a1	14.6	1.2	ATPase, Ca++ transporting, cardiac muscle, fast twitch 1
NM_009405.2	Tnni2	14.2	2.1	troponin I, skeletal, fast 2
NM_011620.2	Tnnt3	13.3	1.5	troponin T3, skeletal, fast
NM_016958.1	Krt14	11.3	2.6	keratin 14
NM_007606.3	Car3	10.2	2.2	carbonic anhydrase 3
NM_007710.2	Ckm	10.1	0.9	creatine kinase, muscle
NM_010859.1	Myl3	8.7	1.6	myosin, light polypeptide 3
NM_013645.3	Pvalb	8.4	0.9	parvalbumin
NM_007702.1	Cidea	8.1	3.8	cell death-inducing DNA fragmentation factor, alpha subunit-like effector A
NM_144936.1	Tmem45b	7.8	3.8	transmembrane protein 45b
NM_025425.3	Rpl3l	7.6	0.8	ribosomal protein L3-like
XM_130312.3	Ttn	7.5	0.8	Titin (known as connectin)
NM_009381.2	Thrsp	7.2	3.5	thyroid hormone responsive SPOT14 homolog
NR_001592.1	H19	7.0	0.9	H19 fetal liver mRNA, non-coding RNA.
NM_011540.2	Tcap	6.6	0.9	titin-cap
NM_007751.2	Cox8b	6.6	1.6	cytochrome c oxidase, subunit VIIIb
NM_007906.2	Eef1a2	6.6	0.9	eukaryotic translation elongation factor 1 alpha 2
NM_013743.2	Pdk4	6.4	2.1	pyruvate dehydrogenase kinase, isoenzyme 4
NM_007906.2	Eef1a2	6.2	0.8	eukaryotic translation elongation factor 1 alpha 2
NM_026384.3	Dgat2	6.2	2.8	diacylglycerol O-acyltransferase 2
NM_013593.2	Mb	5.8	0.8	myoglobin
NM_013459.1	Cfd	5.8	2.7	complement factor D (adipsin)
NM_198415.1	Ckmt2	5.6	0.8	creatine kinase, mitochondrial 2
NM_198415.2	Ckmt2	5.3	0.8	creatine kinase, mitochondrial 2, nuclear gene encoding mitochondrial protein
NM_009605.4	Adipoq	5.3	3.0	adiponectin, C1Q and collagen domain containing
NM_020568.2	S3–12	5.1	1.6	plasma membrane associated protein, S3–12
NM_007933.2	Eno3	5.1	0.7	enolase 3, beta muscle
NM_008469.1	Krt15	5.1	1.0	keratin 15
NM_018870.2	Pgam2	5.0	1.1	phosphoglycerate mutase 2
NM_008726.3	Nppb	5.0	2.8	natriuretic peptide precursor type B
NM_009944.3	Cox7a1	4.9	1.5	cytochrome c oxidase, subunit VIIa 1
NM_001033303.2	Ampd1	4.6	0.4	adenosine monophosphate deaminase 1 (isoform M), XM_921992
NM_007732.1	Col17a1	4.4	1.0	collagen, type XVII, alpha 1
NM_033268.3	Actn2	4.4	0.7	actinin alpha 2
NM_145635.2	BC054059	4.3	1.9	cDNA sequence BC054059
NM_198059.2	Nrap	4.2	0.4	nebulin-related anchoring protein, transcript variant 1
NM_009109.2	Ryr1	4.1	0.3	ryanodine receptor 1, skeletal muscle
NM_009948.1	Cpt1b	4.1	1.4	carnitine palmitoyltransferase 1b, muscle
NM_001012401.1	Hspb6	4.1	0.6	heat shock protein, alpha-crystallin-related, B6
NM_025540.2	Sln	4.1	0.9	Sarcolipin
NM_010174.1	Fabp3	4.0	1.2	fatty acid binding protein 3, muscle and heart
NM_011641.1	Trp63	4.0	0.9	transformation related protein 63
NM_001079932.1	Trim72	4.0	0.6	tripartite motif-containing 72

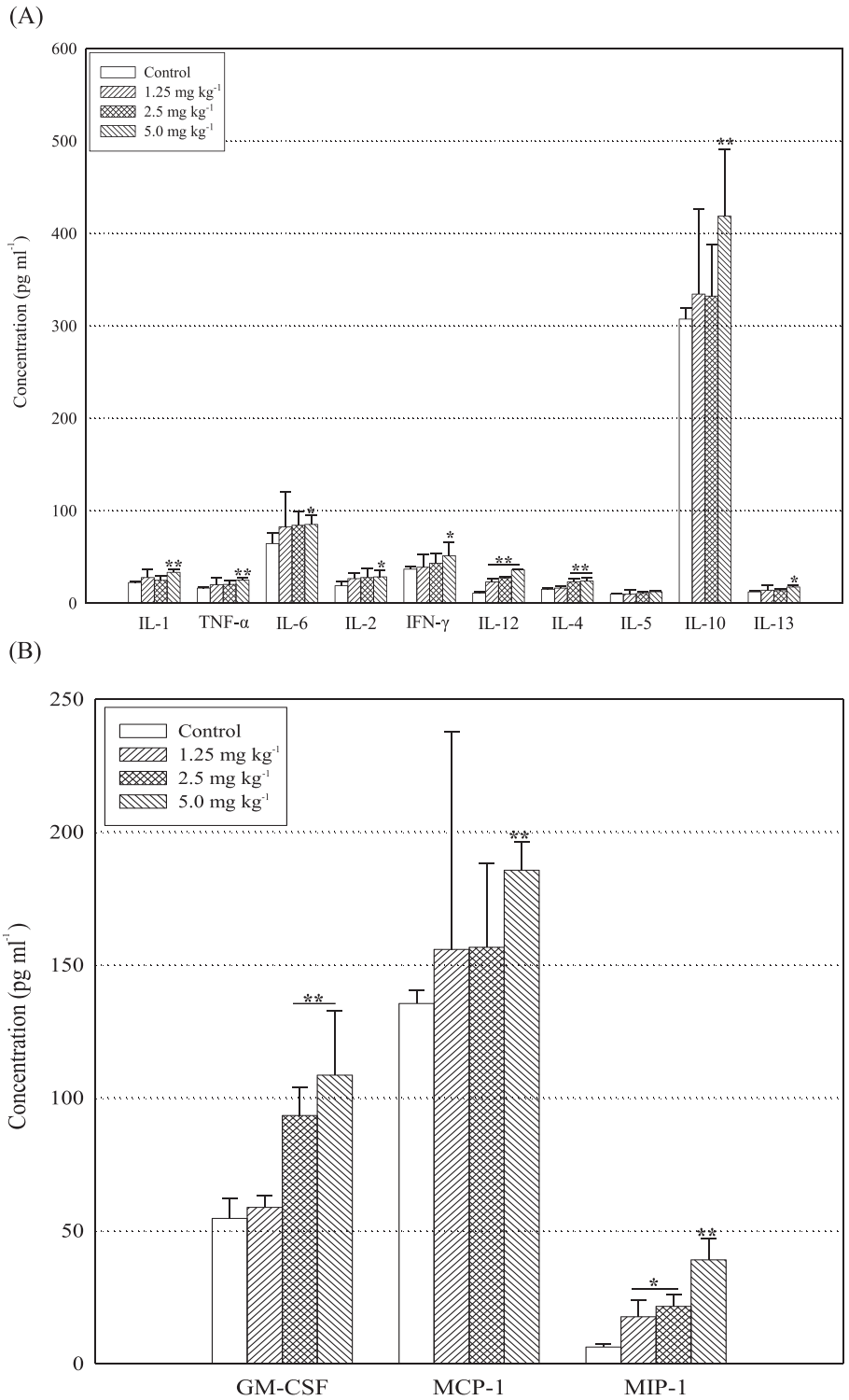

Figure 5. The effects of graphene nanoplatelet (GNP) accumulation on inflammatory mediators in the lung. After centrifuging, the supernatants of BAL fluids (eight mice per group) were used for each assay (100 μl per well per mouse, $n = 8$). The values were calculated using a standard curve, which was made under the same condition. Data show the mean ± SD. *$P < 0.05$, **$P < 0.01$. (A) Changes in inflammatory cytokines, (B) changes in chemokines.

encoding actin family cytoskeletal proteins, including Myh 8, Acta1, Mylpf, Tpm2, Tnnt3 and Krt14, were enhanced notably in the lungs of the GNP-treated mice (5 mg kg^{-1}; Table 1), expression of genes encoding calcium-binding proteins, such as Tnnc2, Myl1, Myl3, and Pvalb, was also significantly enhanced by pulmonary accumulation of GNP. Also, interestingly, the expression of natriuretic-related genes was noteworthy altered. While expression of H2-Ea, a major histocompatibility complex (MHC) class II protein, markedly decreased (−4.9 ± 3.7 fold, Table 2), that of Cd8b1, which binds MHC class I proteins, clearly increased (3.5 ± 2.3 fold), as

Journal of Applied Toxicology

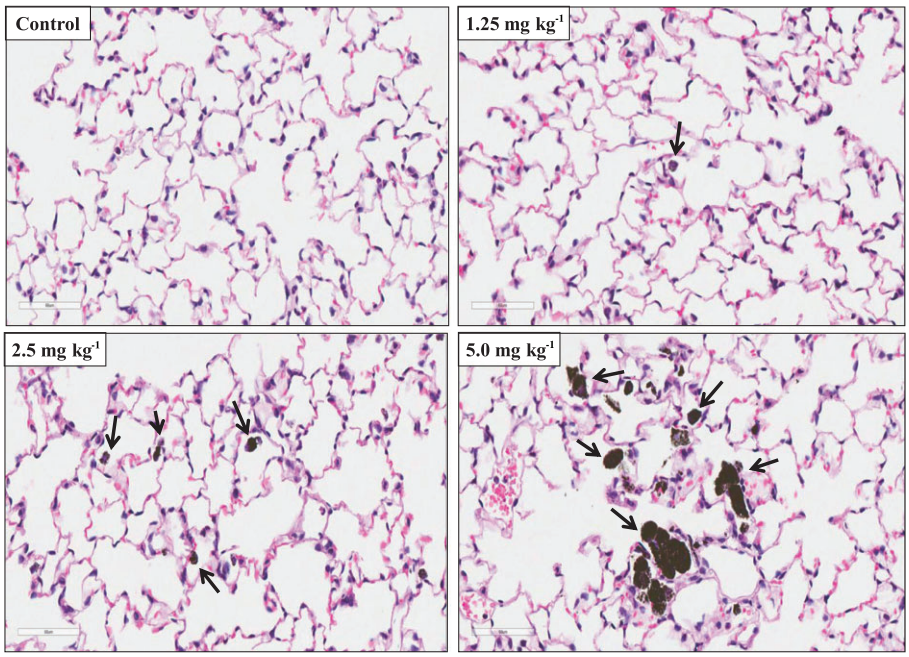

Figure 6. Histopathological changes after graphene nanoplatelet (GNP) accumulation. A representative image by dose was suggested. Arrows indicate pulmonary persistence of GNP.

Table 2. A list of down-regulated genes after graphene nanoplatelet (GNP) accumulation. A list shows genes, which were down-regulated more than two-fold with statistical significance ($P < 0.05$)

RefSeq_NM	GeneSymbol	Fold	SD	DEFINITION
NM_030560.3	BC003993	−2.9	3.4	cDNA sequence BC003993
NM_009263.1	Spp1	−2.9	1.0	secreted phosphoprotein 1
NM_010381.2	H2-Ea	−4.9	3.7	histocompatibility 2, class II antigen E alpha
NM_007791.4	Csrp1	−6.4	3.1	cysteine and glycine-rich protein 1

compared with the control. Moreover, expression of the secreted phosphoprotein 1 (Spp1) gene, known as early T-lymphocyte activation-1 or osteopontin, notably decreased (−2.9 ± 1.0 fold, Ashkar *et al*., 2000; Wang and Denhardt, 2008; Kaleta, 2014).

GNPs induced hematological and biochemical imbalance in the bloodstream

At the 5-mg kg^{-1} dose, the number of white blood cells (WBC), the percentage of macrophages and neutrophils (Table 3) and the production of IgG, IgM and IgA, but not IgE (Fig. 7), were significantly elevated compared with the control. Additionally, in the same group, total protein, BUN and potassium levels notably decreased compared with the control (Table 4).

GNP systemically augmented the distribution of B and helper T cells, inhibiting function of antigen-presenting cells

The spleen plays an important role in immune function and erythrocytes, and splenocytes consist of various cell populations, including lymphocytes, dendritic cells and macrophages. Here, we analyzed the systemic immunotoxic effect after pulmonary persistence of GNP using splenocytes from each group. The B cell distribution and the relative ratio of helper T cells to cytotoxic T cells increased in mice exposed to the highest dose of GNP compared with the control (Fig. 8A). In the control and 5-mg kg^{-1} groups, the distribution of B cells was 69.2 ± 3.6 and 78.2 ± 2.6%, respectively, and the relative ratio of helper T cells to cytotoxic T cells was 3.5 ± 0.4 and 4.8 ± 1.4, respectively. Also, proliferation and activation of B cells depend on signals from helper T cells, phagocytic cells, and professional antigen-presenting-cells (APCs), and APCs suggest information on antigen with CD80, CD86, CD40 and MHC class II (MII) molecules on their surface. In this study, expression of MHC class II protein tended to increase on splenocytes (Total MII), B cells (MII/$CD19^+$) and mature dendritic cells (MII/$CD11c^+$), expression of CD40 was also enhanced on splenocytes (Total CD40) and B cells ($CD40^+$/$CD19^+$; Fig. 8B). Meanwhile, expression of CD40 on mature dendritic cells ($CD40^+$/$CD11c^+$) and co-expression of CD86 and CD80 on splenocytes ($CD86^+$/$CD80^+$) was attenuated compared to the control. While the proportion of regular ($CD11b^+$/$CD11c^-$) and immature dendritic cells ($CD11b^+$/$CD11c^+$) significantly decreased at a 5-mg kg^{-1} dose compared with the control, the proportion of mature dendritic cells ($CD11b^-$/$CD11c^+$) increased. Also, as compared with the control, expression of CD22, a surface marker of activated B cells, was enhanced in the GNP-treated groups, expressions of chemotaxis-related proteins, such as CCR5 and CXCR2, also increased (Fig. 8C).

Table 3. Hematological changes after graphene nanoplatelet (GNP) accumulation. Eight samples per group were measured.

Name	WBC	LY	MO	NE	EO	BA	RBC	MCV	HCT	MCH	MCHC	Hgb	RDW	PLT	MPV
Uint	K/uL	%	%	%	%	%	M/uL	fL	%	pg	g/dL	g/dL	%	K/uL	fL
Control	2.2 ± 0.2	85.8 ± 1.7	4.4 ± 1.7	8.0 ± 1.1	0.6 ± 0.3	0.4 ± 0.3	8.4 ± 0.3	53.7 ± 1.0	46.2 ± 2.9	16.3 ± 0.6	31.2 ± 2.1	13.4 ± 1.2	18.0 ± 0.6	837.4 ± 71.0	8.0 ± 0.6
1.25 mg/kg	2.9 ± 1.2	82.4 ± 1.9	6.0 ± 1.7	9.5 ± 1.5	0.8 ± 0.6	0.5 ± 0.2	8.5 ± 0.8	54.5 ± 2.1	45.0 ± 4.7	16.5 ± 0.7	30.2 ± 1.5	14.2 ± 0.8	17.7 ± 0.6	912.5 ± 78.3	8.1 ± 0.7
2.5 mg/kg	3.2 ± 1.3	74.2 ± 8.2**	8.8 ± 3.3	17.2 ± 4.6**	0.7 ± 0.5	0.8 ± 0.1*	8.2 ± 0.3	52.3 ± 1.6	43.0 ± 0.8	16.4 ± 0.7	31.4 ± 1.1	13.5 ± 0.3	18.0 ± 0.4	905.6 ± 60.5	8.1 ± 0.3
5.0 mg/kg	3.8 ± 1.4*	69.1 ± 8.7**	9.1 ± 2.5**	19.6 ± 7.9**	2.0 ± 2.2	0.7 ± 0.1	8.1 ± 0.6	51.5 ± 2.1	42.5 ± 5.3	16.9 ± 0.8	32.6 ± 2.1	14.3 ± 1.6	18.3 ± 0.6	862.6 ± 65.8	8.8 ± 0.7

* $P < 0.05$,
** $P < 0.01$.
WBC, white blood cells; LY, lymphocytes; MO, monocytes; NE, neutrophils; EO, eosinophils; BA, basophils; RBC, red blood cells; MCV, mean corpuscular volume; HCT, hematocrit; MCH, mean corpuscular hemoglobin; MCHC, mean corpuscular hemoglobin concentration;Hgb, hemoglobin; RDW, red blood cell distribution width; PLT, platelet; MPV, mean platelet volume

Discussion

Recently, some researchers suggested that studies on the long-term toxicological and metabolic behaviors of grapheme-based nanomaterials are needed for their clinical use (Yang *et al.*, 2013; Nezakati *et al.*, 2014). Graphene and its derivatives include mono- or multilayer graphene, GO, reduced GO and graphene nanosheets, which vary in shape, size, surface area, the number of layers, chemical modifications and other characteristics. Most engineers are trying to produce the highest quality of graphene sheets for application in industry such as energy storage. However, we should simultaneously consider that surface area, layer number, lateral dimension, surface chemistry and purity are the important properties that affect the biological effects of graphene and its derivatives (Duch *et al.*, 2011; Kotchey *et al.*, 2011; Girish *et al.*, 2013; Braakhuis *et al.*, 2014; Guo and Mei, 2014; Kostarelos and Novoselov, 2014; Schinwald *et al.*, 2014). For example, when treated to liver hepatocellular carcinoma cells, a significant decrease in cell viability was induced by 0.5 $\mu g\,ml^{-1}$ graphene and 20 $\mu g\,ml^{-1}$ GO (Liu *et al.*, 2016). In contrast, the plate-like graphene shells and graphene oxide paper was non-toxic in Escherichia coli, whereas GO was toxic (EC_{50} of $1.13 \pm 0.05 \times 10^{-4}$ $\mu g\,ml^{-1}$ after exposure, Efremova *et al.*, 2015). Additionally, owing to their differential surface oxidation status, hydrophilic GO showed a high deregulation of antioxidant-, DNA repair- and apoptosis-related genes with notable cellular uptake, whereas hydrophobic rGO mostly adsorbed at cell surface accompanying poor gene regulation (Chatterjee *et al.*, 2014). In this study, we used GNP with a thickness corresponding to the stacking of approximately 10 layers of monatomic graphene sheets with considerably few defects (Park *et al.*, 2015a).

The uptake level, biodegradation and bioaccumulation of nanomaterials are important in determining their safety and considering their application in biomedicine (Braakhuis *et al.*, 2014; Rahman *et al.*, 2015). According to the previous reports, graphene more easily internalizes into the cell than other materials that are large and have smooth surfaces, owing to its small size, sharp edges and rough surfaces. Also, graphene is resistant to degradation because of its excellent electronic transport properties and high surface-to-volume ratios (Guo and Mei, 2014). For instance, graphene easily entered the body via the unusual routes and induced a phagocytic immune response *in vivo* and *in vitro*, despite insufficient phagocytosis (Schinwald *et al.*, 2012; Li *et al.*, 2013; Qu *et al.*, 2013; Chen *et al.*, 2014). Similarly, graphene spontaneously penetrates the cell membrane at edge asperities and corner sites (Li *et al.*, 2013), and GO and carboxyl GNP penetrate through the plasma membrane into the cytosol (Lammel *et al.*, 2013). As well, pristine, multi-layered GNP was not oxidized in the lungs of mice and was relatively stable in the presence of enzymes. Moreover, in our previous study, GNP located within autophagosome-like vacuoles in human bronchial epithelial cells at 24 h after exposure and remained in the lung on day 28 after a single intratracheal instillation (Park *et al.*, 2015a). Similarly, in this study, GNP was still located within the lung on day 90 after a single intratracheal instillation.

Our body contains three primary cytoskeletal filaments: microfilaments, intermediate filaments and microtubules. These proteins are very important to maintain the structure, shape and normal function of cells, including muscle contraction, cell division, cell signaling and cell mobility. Increasing studies have shown that cytoskeletal damage is an important adverse effect caused by graphene exposure. For example, GO attenuated the

Journal of Applied Toxicology

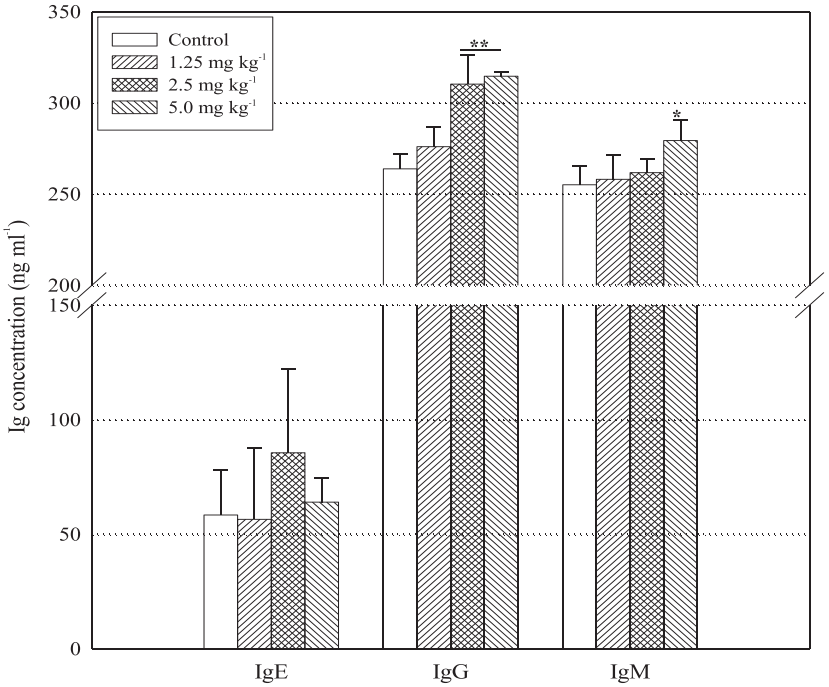

Figure 7. Alteration in immunoglobuline production. A serum was diluted at a ratio of 1000:1 according to the manufacturer's instructions. The assay was performed using four wells per sample. Values express the mean ± SD. *$P < 0.05$, **$P < 0.01$.

viability and function of macrophages via cytoskeletal damage and oxidative stress (Qu *et al*., 2013; Tu *et al*., 2013). Additionally, GO and carboxyl GNP induced structural damage because of their high affinity to the plasma membrane (Lammel *et al*., 2013). Additionally, some studies reported an alteration in metabolic activity through mitochondrial damage caused by graphene exposure (Lammel *et al*., 2013; Rahman *et al*., 2015; Chen *et al*., 2015). Similarly, in our previous study, GNP suppressed ATP production by impairing the mitochondrial function in human bronchial epithelial cells (Park *et al*., 2015a). As well, in this study, the mitochondrial damage was observed in the TEM images of the lung collected on day 90 after a single instillation of GNP (5 -mg kg^{-1} dose). Moreover, in this study, upregulation of skeletal-, calcium binding- and natriuretic-related genes and a significant decrease in total protein, BUN and potassium levels were observed in the lung and the blood of mice exposed to the highest dose, respectively. Skeletal muscle myosin enzymatic activity is required for pulmonary myofibroblast contractility (Walker *et al*., 2001; Rice and Leinwand, 2003), and increased intracellular calcium has a notable effect on the activity of the adult fast myosin heavy chain promoters (Allen and Leinwand, 2002). Additionally, low serum potassium promotes the development of diabetes and increases the risk of lethal ventricular arrhythmias in patients with ischaemic heart disease, heart failure and left ventricular hypertrophy (He and MacGregor, 2008), and increased urinary Na^+ excretion and urine volume are exhibited in natriuresis (Zhou *et al*., 2013). Herein, we feel that further study is necessary to assess the effects of GNP exposure on the physiological condition (Park *et al*., 2015b, 2016).

The human body consists of approximately 37 trillion cells, which have different functions, these cells are constantly dying accidentally or by natural process, and dead cells can act as inflammatory or immunogenic stimuli as well as foreign substances (Maderna and Godson, 2003; Chung *et al*., 2006; Kindt *et al*., 2006; Park *et al*., 2015b, 2016). Thus, the immune cells have to remove dead or dying cells rapidly by phagocytosis, and both professional and non-professional phagocytes play an important role in this process. Macrophages, neutrophils and dendritic cells are typical professional phagocytes, and these professional phagocytes recruit immune cells into the inflammatory site by secreting a variety of cytokines and chemokines. In our previous study, GNP induced a dose-dependent decrease in cell viability and an increase in the number of cells in the subG1 region and S phase (Park *et al*., 2015a). As well, in this study, the generation of apoptotic cells (approximately sevenfold of the control at 5-mg kg^{-1} dose) and recruitment of immune cells, especially lymphocytes, into the lungs were observed in the GNP-treated mice along with an elevated distribution of neutrophils and macrophages and an increased number of WBCs in the blood. Also, GNP-laden macrophages were markedly observed in the lungs of the treated mice with an enhanced secretion of GM-CSF. Moreover, GNP (5 mg kg^{-1}) notably enhanced the expression of the gene encoding the antigen for $CD8^+$ T cells, which recognizes MHC class I molecules, and inhibited the expression of Spp1 gene, an important anti-apoptotic factor (Khan *et al*., 2002), accompanied by a remarkable decrease in the expression of the H2-Ea gene, a MHC class II protein component. The killing effect of macrophages and the activation of cytotoxic ($CD8^+$) T cells are augmented in Th1-type immune responses (Luther and Cyster, 2001; Kindt *et al*., 2006). Also, GM-CSF, a WBC growth factor, is secreted by macrophages and T lymphocytes and stimulates the production of monocytes and granulocytes, such as neutrophils, eosinophils and basophils (Francisco-cruz *et al*., 2014). Moreover, E2-Ea deficiency is a risk factor for lung fibrosis (Du *et al*., 2004), and Spp1 deficiency results in a reduced Th1 immune response

Table 4. Blood biochemical changes after graphene nanoplatelet (GNP) accumulation. Six samples per group were used for analysis.

Name	Total protein	Albumin	Total Bilirubin	Glucose	BUN	Creatinine	AST	ALT	ALP	γ-GTP	Amylase	Sodium	Potassium	Chloride	Globulin
Unit	g/dL	g/dL	mg/dL	mg/dL	mg/dL	mg/dL	U/L	U/L	U/L	U/L	U/L	mmol/L	mmol/L	mmol/L	g/dL
Control	4.6 ± 0.2	3.3 ± 0.1	0.0 ± 0.1	255.7 ± 40.1	29.2 ± 3.2	0.3 ± 0.0	58.5 ± 20.1	35.3 ± 10.8	51.0 ± 5.6	0.0 ± 0.0	3655.8 ± 214.0	141.8 ± 2.3	8.1 ± 1.0	112.4 ± 1.5	1.2 ± 0.1
1.25 mg/kg	4.2 ± 0.2*	3.2 ± 0.1	0.1 ± 0.0	264.7 ± 34.8	26.3 ± 3.4	0.3 ± 0.0	78.2 ± 13.3	53.0 ± 12.8	48.7 ± 6.7	0.0 ± 0.0	3478.4 ± 414.3	143.6 ± 1.4	5.7 ± 0.7**	114.7 ± 2.7	1.0 ± 0.1
2.5 mg/kg	4.2 ± 0.2*	3.3 ± 0.2	0.1 ± 0.0	277.2 ± 30.0	23.8 ± 2.7*	0.2 ± 0.1	82.2 ± 13.2	68.3 ± 17.4**	40.8 ± 5.5	0.0 ± 0.0	3491.9 ± 441.0	143.4 ± 0.7	5.6 ± 0.8**	112.7 ± 1.4	1.0 ± 0.1
5.0 mg/kg	4.2 ± 0.1**	3.3 ± 0.2	0.1 ± 0.0	308.2 ± 40.9	21.6 ± 4.4*	0.3 ± 0.1	88.2 ± 18.9	80.2 ± 47.3	54.8 ± 21.5	0.0 ± 0.0	3674.6 ± 335.9	143.9 ± 0.9	5.3 ± 0.4**	112.5 ± 0.9	1.0 ± 0.1

* $P < 0.05$,
** $P < 0.01$.
AST; aspartate aminotransferase, ALT; alanine aminotransferase, ALP; alkaline phosphatase, γ-GTP; gamma-glutamyl transferase.

in infectious diseases, autoimmunity and delayed type hypersensitivity (Wang and Denhardt, 2008; Kaleta, 2014). Here, we suggest that alteration in immune regulation after pulmonary persistence of GNP may contribute, in part, to the generation of dead and damaged cells. In addition, we feel that further studies are required to evaluate the possibility of lung fibrosis after chronic exposure to GNP.

Recently, some researchers emphasized that imbalance of the immune system is a side effect of exposure to graphene (Di Gioacchino *et al.*, 2011; Chen *et al.*, 2014). Moreover, pulmonary nanoparticles can induce a systemic immune response as well as a local immune response by translocating via the blood stream and lymphatic system. In this study, the distribution of B cells and helper T cells was dominant in splenocytes, and expression of CD40 protein was enhanced on splenocytes and B cells with an increase in the number of activated B cells. However, the expression of CD40 protein clearly decreased in mature dendritic cells, and that of MHC class II protein did not show a significant change in mice exposed to GNP. More importantly, the co-expression of CD80 and CD86 obviously decreased on the surface of splenocytes. B cells cannot phagocytose the antigen itself despite being professional APCs. Therefore, the bridge-building role of professional phagocytes or non-professional phagocytes such as epithelial cells, endothelial cells and fibroblasts are required for activation and proliferation of B cells. In addition, helper T cells recognize and interact with the antigen in the complex with MHCs on APCs, but not the antigen itself, by using their T-cell receptors, and professional APCs, including dendritic cells, macrophages and B cells, can carry information from the antigen to other cells by expressing co-stimulatory markers, including MHC class II and CD40 proteins, with both CD80 and CD86 proteins on their membranes (Mackey *et al.*, 1998; Zou and Tam, 2002; Zhu and Paul, 2008; Zhang *et al.*, 2014c). Moreover, CD195, known as CCR5, is expressed on T cells, macrophages, dendritic cells and eosinophils, and MIP-1α and -1β bind to this receptor (Menten *et al.*, 2002; Wong and Fish, 2003). CXCR2 is also expressed on neutrophils and binds to IL-8. In this study, expressions of CD195 and CXCR2 significantly increased in mice exposed to GNP compared with the control. Considering that humans are continuously exposed to xenobiotics and that both innate and adaptive immunity are initiated by uptake and processing of antigen by resident- and recruited immune cells, we suggest that persistence of GNP may influence a host's defensive abilities on the attack of a foreign body by suppressing the function of APCs. Furthermore, in our previous studies, iron oxide nanoparticles (2 mg kg^{-1}) and single-walled carbon nanotubes (200 μg kg^{-1}) induced a stronger Th1-polarized immune response with higher IL-12 level on day 90 after instillation compared with GNP (5 mg kg^{-1}). Considering that expression of IFN-γ and CD40L is important for IL-12 production and DC activation, leading to cytotoxic T cell stimulation, and that the expression of CD40 protein clearly decreased on mature dendritic cells in this study, we suggest the need for the further study of the effects of GNP on DC function and T cell exhaustion, especially the cytotoxic T cell (Loskog *et al.*, 2006; Rodrigue-Gervais *et al.*, 2010; Hansen *et al.*, 2012).

In conclusion, we found that pulmonary persistence of GNP induced Th1-shifted immune responses with cytoskeletal damage in the lung and systemically suppressed the function of APCs. Also, we suggest that persistence of GNP may cause adverse health effects by impairing physiological homeostasis.

Journal of Applied Toxicology

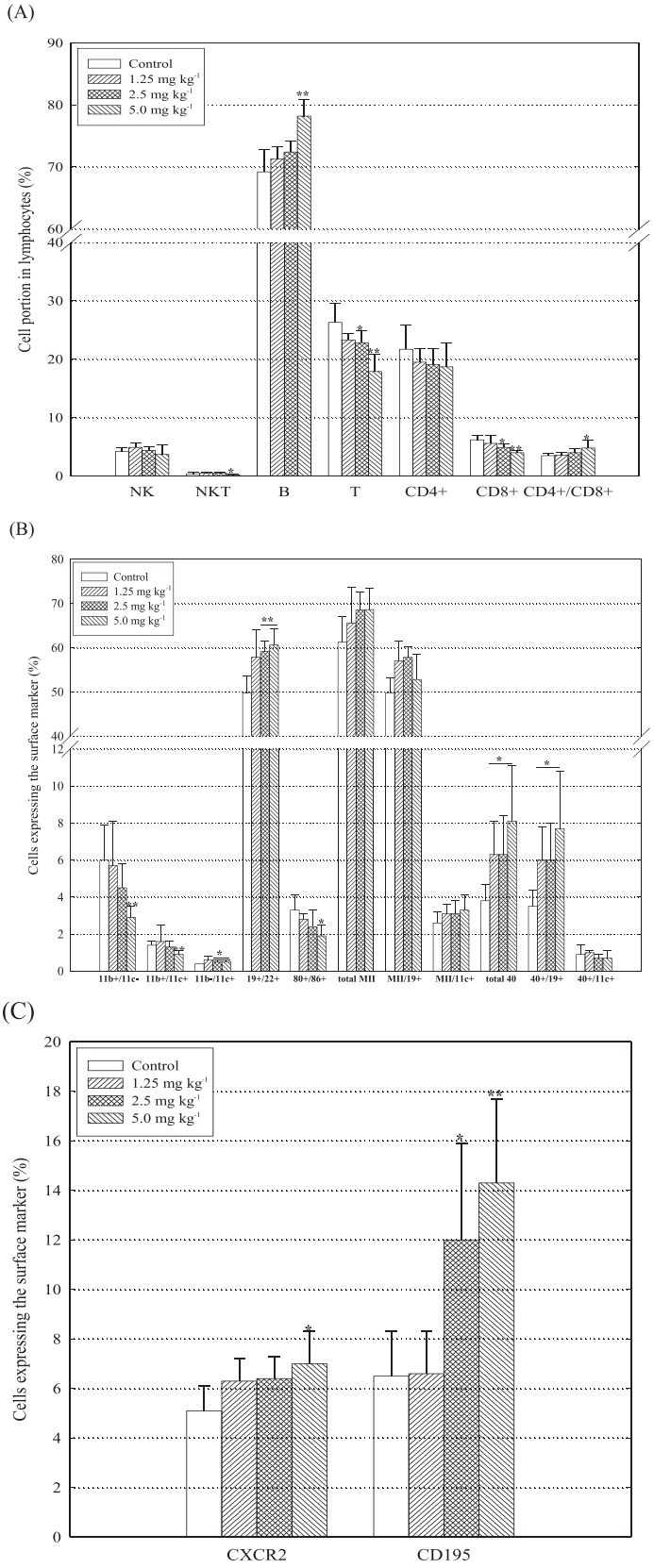

Figure 8. The effects of graphene nanoplatelet (GNP) accumulation on the systemic immune response. After blocking with Fc-block antibody (CD16), splenocytes (8 samples/group) were stained in the dark with directly conjugated monoclonal antibody for 30 min at 4 °C. 10 000 cells per sample were counted. Values express the mean ± SD. *$P < 0.05$, **$P < 0.01$. (A) Distribution of lymphocyte components, (B) Expression of antigen-presenting related-surface markers. In 'CD name' of each protein, front letters 'CD' was omitted. MII: MHC class II, 11b+/11c-, regulatory DCs, 11b+/11c+, immature DCs; 11b−/11c+, mature DCs. (C) Expression of chemokine receptors.

Acknowledgements

This work was supported by the Basic Science Research Program through the National Research Foundation of Korea funded by the Ministry of Education, Science and Technology (2011-35B-E00011).

Conflict of interest

The authors report no declarations of interest.

References

Ali-Boucetta H, Bitounis D, Raveendran-Nair R, Servant A, Van den Bossche J, Kostarelos K. 2013. Purified graphene oxide dispersions lack in vitro cytotoxicity and in vivo pathogenicity. *Adv. Healthc. Mater.* **2**: 433–441.

Allen DL, Leinwand LA. 2002. Intracellular calcium and myosin isoform transitions. Calcineurin and calcium-calmodulin kinase pathways regulate preferential activation of the IIa myosin heavy chain promoter. *J. Biol. Chem.* **277**: 45323–45330.

Ashkar S, Weber GF, Panoutsakopoulou V, Sanchirico ME, Jansson M, Zawaideh S, Rittling SR, Denhardt DT, Glimcher MJ, Cantor H. 2000. Eta-1(osteopontin): an early component of type-1(cell-mediated) immunity. *Science* **287**: 860–864.

Braakhuis HM, Park MV, Gosens I, De Jong WH, Cassee FR. 2014. Physicochemical characteristics of nanomaterials that affect pulmonary inflammation. *Part. Fibre Toxicol.* **11**: 18.

Bussy C, Ali-Boucetta H, Kostarelos K. 2013. Safety considerations for graphene: Lessons learnt from carbon nanotubes. *Acc. Chem. Res.* **46**: 692–701.

Campbell JD, HayGlass KT. 2000. T cell chemokine receptor expression in human Th1- and Th2-associated diseases. *Arch. Immunol. Ther. Exp.* **48**: 451–456.

Chatterjee N, Eom HJ, Choi J. 2014. A systems toxicology approach to the surface functionality control of graphene-cell interactions. *Biomaterials* **35**: 1109–1127.

Chen GY, Chen CL, Tuan HY, Yuan PX, Li KC, Yang HJ, Hu YC. 2014. Graphene oxide triggers toll-like receptors/autophagy responses in vitro and inhibits tumor growth in vivo. *Adv. Healthc. Mater.* **3**: 1486–1495.

Chen Y, Hu X, Sun J, Zhou Q. 2015. Specific nanotoxicity of graphene oxide during zebrafish embryogenesis. Nanotoxicology Epub ahead of print.

Chung EY, Kim SJ, Ma XJ. 2006. Regulation of cytokine production during phagocytosis of apoptotic cells. *Cell Res.* **16**: 154–161.

Colantonio L, Recalde H, Sinigaglia F, D'Ambrosio D. 2002. Modulation of chemokine receptor expression and chemotactic responsiveness during differentiation of human naive T cells into Th1 or Th2 cells. *Eur. J. Immunol.* **32**: 1264–1273.

Di Gioacchino M, Petrarca C, Lazzarin F, Di Giampaolo L, Sabbioni E, Boscolo P, Mariani-Costantini R, Bernardini G. 2011. Immunotoxicity of nanoparticles. *Int. J. Immunopathol. Pharmacol.* **24**(1 Suppl.): 65S–71S.

Du M, Irani RA, Stivers DN, Lee SJ, Travis EL. 2004. H2-Ea deficiency is a risk factor for bleomycin-induced lung fibrosis in mice. *Cancer Res.* **64**: 6835–6839.

Duch MC, Budinger GR, Liang YT, Soberanes S, Urich D, Chiarella SE, Campochiaro LA, Gonzalez A, Chandel NS, Hersam MC, Mutlu GM. 2011. Minimizing oxidation and stable nanoscale dispersion improves the biocompatibility of graphene in the lung. *Nano Lett.* **11**: 5201–5207.

Efremova LV, Vasilchenko AS, Rakow EG, Deryabin DG. 2015. Toxicity of graphene shells, graphene oxide, and graphene oxide paper evaluated with Escherichia coli Biotests. *Biomed. Res. Int.* **2015**: 869361.

Francisco-Cruz A, Aguilar-Santelises M, Ramos-Espinosa O, Mata-Espinosa D, Marquina-Castillo B, Barrios-Payan J, Hernandez-Pando R. 2014. Granulocyte-macrophage colony-stimulating factor: not just another haematopoietic growth factor. *Med. Oncol.* **31**: 774.

Geim AK. 2009. Graphene: status and prospects. *Science* **324**: 1530–1534.

Goenka S, Sant V, Sant S. 2014. Graphene-based nanomaterials for drug delivery and tissue engineering. *J. Control. Release* **173**: 75–88.

Girish CM, Sasidharan A, Gowd GS, Nair S, Koyakutty M. 2013. Confocal Raman imaging study showing macrophage mediated biodegradation of graphene in vivo. *Adv. Healthc. Mater.* **2**: 1489–1500.

Guo X, Mei N. 2014. Assessment of the toxic potential of graphene family nanomaterials. *J. Food Drug Anal.* **22**: 105–115.

Hansen M, Met Ö, Svane IM, Andersen MH. 2012. Cellular based cancer vaccine: type 1 polarization of dendritic cells. *Curr. Med. Chem.* **19**: 4239–4246.

He FJ, MacGregor GA. 2008. Beneficial effects of potassium on human health. *Physiol. Plant.* **133**: 725–735.

Kaleta B. 2014. Role of osteopontin in systemic lupus erythematosus. *Arch. Immunol. Ther. Exp.* **62**: 475–482.

Khan SA, Lopez-Chua CA, Zhang J, Fisher LW, Sørensen ES, Denhardt DT. 2002. Soluble osteopontin inhibits apoptosis of adherent endothelial cells deprived of growth factors. *J. Cell. Biochem.* **85**: 728–736.

Kim CH, Rott L, Kunkel EJ, Genovese MC, Andrew DP, Wu L, Butcher EC. 2001. Rules of chemokine receptor association with T cell polarization in vivo. *J. Clin. Invest.* **108**: 1331–1339.

Kindt TJ, Osborne BA, Goldsby RA. 2006. *Kuby Immunology*, 6th edn. W.H. Freeman & Company: London, UK.

Kostarelos K, Novoselov KS. 2014. Materials science. Exploring the interface of graphene and biology. *Science* **344**: 261–263.

Kotchey GP, Allen BL, Vedala H, Yanamala N, Kapralov AA, Tyurina YY, Klein-Seetharaman J, Kagan VE, Star A. 2011. The enzymatic oxidation of graphene oxide. *ACS Nano* **5**: 2098–2108.

Kuila T, Mishra AK, Khanra P, Kim NH, Lee JH. 2013. Recent advances in the efficient reduction of graphene oxide and its application as energy storage electrode materials. *Nanoscale* **5**: 52–71.

Lammel T, Boisseaux P, Fernández-Cruz ML, Navas JM. 2013. Internalization and cytotoxicity of graphene oxide and carboxyl graphene nanoplatelets in the human hepatocellular carcinoma cell line Hep G2. *Part. Fibre Toxicol.* **10**: 27.

Li Y, Yuan H, Von dem Bussche A, Creighton M, Hurt RH, Kane AB, Gao H. 2013. Graphene microsheets enter cells through spontaneous membrane penetration at edge asperities and corner sites. *Proc. Natl. Acad. Sci. U. S. A.* **110**: 12295–12300.

Liu S, Jiang W, Wu B, Yu J, Yu H, Zhang XX, Torres-Duarte C, Cherr GN. 2016. Low levels of graphene and graphene oxide inhibit cellular xenobiotic defense system mediated by efflux transporters. *Nanotoxicology* **10**: 597–606.

Loskog A, Ninalga C, Tötterman TH. 2006. Dendritic cells engineered to express CD40L continuously produce IL-12 and resist negative signals from Tr1/Th3 dominated tumors. *Cancer Immunol. Immunother.* **55**: 588–597.

Luther SA, Cyster JG. 2001. Chemokines as regulators of T cell differentiation. *Nat. Immunol.* **2**: 102–107.

Mackey MF, Barth RJ, Jr, Noelle RJ. 1998. The role of CD40/CD154 interactions in the priming, differentiation, and effector function of helper and cytotoxic T cells. *J. Leukoc. Biol.* **63**: 418–428.

Maderna P, Godson C. 2003. Phagocytosis of apoptotic cells and the resolution of inflammation. *Biochim. Biophys. Acta* **1639**: 141–151.

Marques MRC, Loebenberg R, Almukainzi M. 2011. Simulated biological fluids with possible application in dissolution testing. *Dissolut. Technol.* **8**: 15–28.

Menten P, Wuyts A, Van Damme J. 2002. Macrophage inflammatory protein-1. *Cytokine Growth Factor Rev.* **13**: 455–481.

Nezakati T, Cousins BG, Seifalian AM. 2014. Toxicology of chemically modified graphene-based materials for medical application. *Arch. Toxicol.* **88**: 1987–2012.

Novoselov KS. 2011. Graphene: materials in the Flatland (Nobel lecture). *Angew. ChemInt. Ed. Engl.* **50**: 6986–7002.

Park EJ, Lee GH, Han BS, Lee BS, Lee S, Cho MH, Kim JH, Kim DW. 2015a. Toxic response of graphene nanoplatelets in vivo and in vitro. *Arch. Toxicol.* **89**: 1557–1568.

Park EJ, Oh SY, Lee SJ, Lee K, Kim Y, Lee BS, Kim JS. 2015b. Chronic pulmonary accumulation of iron oxide nanoparticles induced Th1-type immune response stimulating the function of antigen-presenting cells. *Environ. Res.* **143**(Pt A): 138–147.

Park EJ, Hong YS, Lee BS, Yoon C, Jeong U, Kim Y. 2016. Single-walled carbon nanotubes disturbed the immune and metabolic regulation function 13-weeks after a single intratracheal instillation. *Environ. Res.* **148**: 184–195.

Perrozzi F, Prezioso S, Ottaviano L. 2015. Graphene oxide: from fundamentals to applications. *J. Phys. Condens. Matter* **27**: 013002.

Qu G, Liu S, Zhang S, Wang L, Wang X, Sun B, Yin N, Gao X, Xia T, Chen JJ, Jiang GB. 2013. Graphene oxide induces toll-like receptor 4 (TLR 4)-dependent necrosis in macrophages. *ACS Nano* **7**: 5732–5745.

Rahman M, Ahmad MZ, Ahmad J, Firdous J, Ahmad FJ, Mushtag G, Kamal MA, Akhter S. 2015. Role of graphene nano-composites in cancer therapy: theanostic applications, metabolic fate and toxicity issues. *Curr. Drug Metab.* **16**: 397–409.

Rice NA, Leinwand LA. 2003. Skeletal myosin heavy chain function in cultured lung myofibroblasts. *J. Cell Biol.* **163**: 119–129.
Rodrigue-Gervais IG, Rigsby H, Jouan L, Sauvé D, Sékaly RP, Willems B, Lamarre D. 2010. Dendritic cell inhibition is connected to exhaustion of CD8+ T cell polyfunctionality during chronic hepatitis C virus infection. *J. Immunol.* **184**: 3134–3144.
Ruiz ON, Fernando KA, Wang B, Brown NA, Luo PG, McNamara ND, Vangsness M, Sun YP, Bunker CE. 2011. Graphene oxide: a nonspecific enhancer of cellular growth. *ACS Nano* **5**: 8100–8107.
Sanchez VC, Jachak A, Hurt RH, Kane AB. 2012. Biological interactions of graphene-family nanomaterials: an interdisciplinary review. *Chem. Res. Toxicol.* **25**: 15–34.
Schinwald A, Murphy F, Askounis A, Koutsos V, Sefiane K, Donaldson K, Campbell CJ. 2014. Minimal oxidation and inflammogenicity of pristine graphene with residence in the lung. *Nanotoxicology* **8**: 824–832.
Schinwald A, Murphy FA, Jones A, MacNee W, Donaldson K. 2012. Graphene-based nanoplatelets: a new risk to the respiratory system as a consequence of their unusual aerodynamic properties. *ACS Nano* **6**: 736–746.
Seabra AB, Paula AJ, de Lima R, Alves OL, Durán N. 2014. Nanotoxicity of graphene and graphene oxide. *Chem. Res. Toxicol.* **27**: 159–168.
Shurin MR, Yanamala N, Kisin ER, Tkach AV, Shurin GV, Murray AR, Leonard HD, Reynolds JS, Gutkin DW, Star A, Fadeel B, Savolainen K, Kagan VE, Shvedova AA. 2014. Graphene oxide attenuates Th2-type immune responses, but augments airway remodeling and hyperresponsiveness in a murine model of asthma. *ACS Nano* **8**: 5585–5599.
Tu Y, Lv M, Xiu P, Huynh T, Zhang M, Castelli M, Liu Z, Huang Q, Fan C, Fang H, Zhou R. 2013. Destructive extration of phospholipids from Escherichia coli membranes by graphene nanosheets. *Nat. Nanotechnol.* **8**: 594–601.
Walker GA, Guerrero IA, Leinwand LA. 2001. Myofibroblasts: molecular crossdressers. *Curr. Top. Dev. Biol.* **51**: 91–107.
Wang KX, Denhardt DT. 2008. Osteopontin: role in immune regulation and stress responses. *Cytokine Growth Factor Rev.* **19**: 333–345.
Wang X, Podila R, Shannahan JH, Rao AM, Brown JM. 2013. Intravenously delivered graphene nanosheets and multiwalled carbon nanotubes induce site-specific Th2 inflammatory responses via the IL-33/ST2 axis. *Int. J. Nanomedicine* **8**: 1733–1748.
Wong MM, Fish EN. 2003. Chemokines: attractive mediators of the immune response. *Semin. Immunol.* **15**: 5–14.
Yang K, Feng L, Shi X, Liu Z. 2013. Nano-graphene in biomedicine: theranostic applications. *Chem. Soc. Rev.* **42**: 530–547.
Zhang W, Lee S, McNear KL, Chung TF, Lee S, Lee K, Crist SA, Ratliff TL, Zhong Z, Chen YP, Yang C. 2014a. Use of graphene as protection film in biological environments. *Sci. Rep.* **4**: 4097.
Zhang Y, Petibone D, Xu Y, Mahmood M, Karmakar A, Casciano D, Ali S, Biris AS. 2014b. Toxicity and efficacy of carbon nanotubes and graphene: the utility of carbon-based nanoparticles in nanomedicine. *Drug Metab. Rev.* **46**: 232–246.
Zhang Y, Zhang Y, Gu W, Sun B. 2014c. TH1/TH2 cell differentiation and molecular signals. *Adv. Exp. Med. Biol.* **841**: 15–44.
Zhou L, Liu G, Jia Z, Yang KT, Sun Y, Kakizoe Y, Liu M, Zhou S, Chen R, Yang B, Yang T. 2013. Increased susceptibility of db/db mice to rosiglitazone-induced plasma volume expansion: role of dysregulation of renal water transporters. *Am. J. Physiol. Renal Physiol.* **305**: F1491–F1497.
Zhu J, Paul WE. 2008. CD4 T cells: fates, functions, and faults. *Blood* **112**: 1557–1569.
Zou GM, Tam YK. 2002. Cytokines in the generation and maturation of dendritic cells: recent advances. *Eur. Cytokine Netw.* **13**: 186–199.

Supporting information

Additional supporting information may be found in the online version of this article at the publisher's web site.